Available online at www.sciencedirect.com
ScienceDirect
Journal of Power Sources 179 (2008) 489–496
JOURNAL OF POWER SOURCES
www.elsevier.com/locate/jpowsour

Alcohol electrooxidation at Pt and Pt–Ru sputtered electrodes under elevated temperature and pressurized conditions

Minoru Umeda [a,*], Hiromasa Sugii [b], Isamu Uchida [b]

[a] *Department of Materials Science and Technology, Faculty of Engineering, Nagaoka University of Technology, Kami-Tomioka, Nagaoka 940-2188, Japan*
[b] *Department of Applied Chemistry, Graduate School of Engineering, Tohoku University, Aramaki-Aoba 07, Aoba-ku, Sendai 980-8579, Japan*

Received 7 October 2007; received in revised form 20 December 2007; accepted 8 January 2008
Available online 16 January 2008

Abstract

The electrooxidation properties of methanol and 2-propanol, which are both promising candidates for direct alcohol fuel cells (DAFCs), have been studied under elevated temperature and pressurized conditions. Sputter-deposited Pt and Pt–Ru electrodes were well-characterized and utilized for the electrochemical measurement of the alcohol oxidation at 25–100 °C. The Pt electrode prepared at 600 °C had a flat surface, and the Pt–Ru formed an alloy. The electrochemical measurements were carried out in a gas-tight cell under elevated temperature, which accompanies the pressurized condition. This is a representative example of the DAFC rising temperature operation. As a result, at 25 °C, the onset potential of the 2-propanol oxidation is about 400 mV more negative than that of the methanol oxidation, and current density of the 2-propanol oxidation exceeds that of the methanol oxidation. Conversely, at 100 °C, the methanol oxidation current density overcomes that of 2-propanol, and the onset potentials of the two are almost the same. The highest current density for the methanol oxidation is obtained at the Pt:Ru = 50:50 electrode, whereas at the Pt:Ru = 35:65 for the 2-propanol oxidation. A Tafel plot analysis was employed to investigate the reaction mechanism. For the methanol oxidation, the number of electrons transferred during the rate-determining process is estimated to be 1 at 25 °C and 2 at 100 °C. This suggests that the methanol reaction mechanism differs at 25 and 100 °C. In contrast, the rate-determining process of the 2-propanol oxidation at 25 and 100 °C was expected to be 1-electron transfer which accompanies the proton-elimination reaction to produce acetone. Consequently, it is deduced that methanol and 2-propanol have an advantage under the rising temperature and room temperature operation, respectively.

Keywords: Fuel cell; Direct alcohol; Methanol; 2-Propanol; Electrooxidation mechanism

1. Introduction

Recently, the research and development of direct alcohol fuel cells (DAFCs) have been significantly extended [1–3]. Thus far, most investigations were devoted to direct methanol fuel cells (DMFCs) due to their simple fueling system design. With regard to the anode reaction, methanol oxidation on Pt produces CO, formaldehyde, formic acid, etc., as reaction intermediates [4]. However, the strong adsorption of CO on the Pt surface during methanol oxidation rapidly diminishes the catalytic performance. Ruthenium addition to Pt is known to be an effective way of reducing the CO poisoning effect due to the strong OH adsorptivity of Ru [5] via a bifunctional mechanism [6–15], which reduces the overpotential for the methanol oxidation. Although many Pt-based electrocatalysts have been tested [16–39], there is no sufficient anode catalyst for the DMFC operation at room temperature.

The temperature rising operation from 60 °C to almost 100 °C is an effective method to obtain a high power DMFC. Researchers at the University of Newcastle upon Tyne have reported over 200 mA cm^{-2} at 0.3 V and 80 °C with Pt–Ru electrodes having a platinum loading of 3.0 mg cm^{-2} [40]. The Jet Propulsion Laboratory in the U.S. has reported over 100 mA cm^{-2} at 0.4 V and 60 °C with a platinum loading of 0.5 mg cm^{-2} [40]. In spite of the success of the temperature rising operation, the methanol oxidation reaction has not been appropriately measured by electrochemical techniques.

The electrooxidation of 2-propanol is known to start at much more negative potentials than that of methanol, while there has been relatively little research regarding the 2-propanol

* Corresponding author. Tel.: +81 258 47 9323.
E-mail address: mumeda@vos.nagaokaut.ac.jp (M. Umeda).

0378-7753/$ – see front matter © 2008 Elsevier B.V. All rights reserved.
doi:10.1016/j.jpowsour.2008.01.011

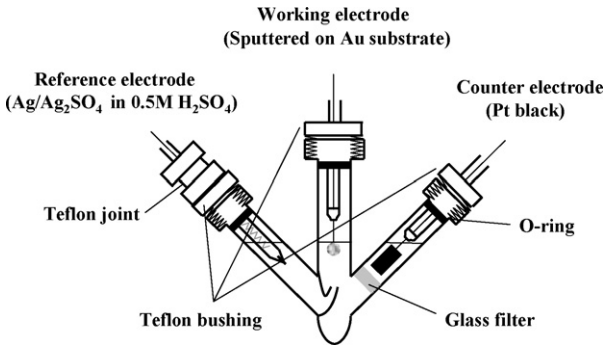

Fig. 1. Schematic illustration of the gas-tight glass cell for electrochemical measurement at elevated temperature.

electrooxidation [41–43]. First, 1-propanol and 2-propanol have different oxidation mechanisms; 1-propanol produces propanal, propionic acid, and CO_2 whereas 2-propanol produces acetone and CO_2. Second, 2-propanol does not produce CO as a reaction intermediate due to the difficulties in carbon chain breaking due to the central positioning of the OH bond in 2-propanol. The absence of CO adsorption during the 2-propanol oxidation leads to a lower oxidation onset potential than in methanol, ethanol, and 1-propanol [41]. As such, 2-propanol is a prospective fuel for DAFCs, as has been suggested in other studies [44–47]. However, the temperature dependence of the electrocatalytic activity and its reaction mechanism have not been fully described [45,48–50].

In the case when we measure the electrochemical oxidation of alcohols in aqueous media, the measuring temperature is limited to 60–70 °C which is attributed to the vaporization of the alcohols. We developed a gas-tight glass cell for the purpose of the electrochemical measurement in alcoholic solutions under elevated temperature which accompanies the pressurized condition based on the alcohol vaporization inside the cell. In the present study, the electrooxidation properties of methanol and 2-propanol were investigated using the well-defined sputtered Pt and Pt–Ru electrodes by varying the temperature of the electrolytic solution. The reaction mechanisms were then discussed from the Tafel slope analyses.

2. Experimental

The 0.5 μm thick electrocatalyst layer was prepared by sputter-deposition on both sides of an Au flag substrate with a 5 mm-diameter and 0.3 mm-thickness. The deposition was performed by a multi-sputter-target machine (Anelva, L-350S-C). The chamber was evacuated to a base pressure of 10^{-4} Pa. The deposition was carried out at a substrate temperature of 600 °C in the chamber filled with 99.999% pure Ar gas to 10 Pa at a substrate rotation speed of 40 rpm. Elemental analysis of the sputter-deposited layer was conducted using an X-ray fluorescence spectrometer (Seiko Instruments, SEA5120). Surface observation of the deposited layer was carried out by a scanning electron microscope (SEM; JEOL, JSM-5310LV). The phase structure was analyzed by an X-ray diffractometer (Shimadzu, XD-D1).

The electrochemical measurements were carried out in a deaerated 0.5 mol dm^{-3} $HClO_4$ + 0.5 mol dm^{-3} alcohol solution. A Pt foil and an Ag/Ag_2SO_4 were used as the counter and reference electrodes, respectively. All potentials reported in this article are with respect to the relative hydrogen electrode (RHE). Cyclic voltammograms (CVs) were measured by a potentiostat (Hokuto Denko, HA-150). Before the experiments in an alcohol-containing solution, the surface of the working electrode was electrochemically cleaned by potential cycling in 0.5 mol dm^{-3} $HClO_4$. The electrochemical impedance spectroscopy (EIS) was measured using a frequency response analyzer (Solartron 1260) in combination with a potentiostat (Solartron 1287).

To investigate the temperature effect of the alcohol electrooxidation, a gas-tight electrochemical cell was employed as is schematically shown in Fig. 1. All the electrodes were connected with glass-sealed lead wires and the chambers were gas-sealed by a screw cap with an O-ring. The cell temperature was controlled from 25 to 100 °C in a forced convection type oven. The inner pressure of the gas-tight cell was measured by a pressure gage (Keller, PR-25HT).

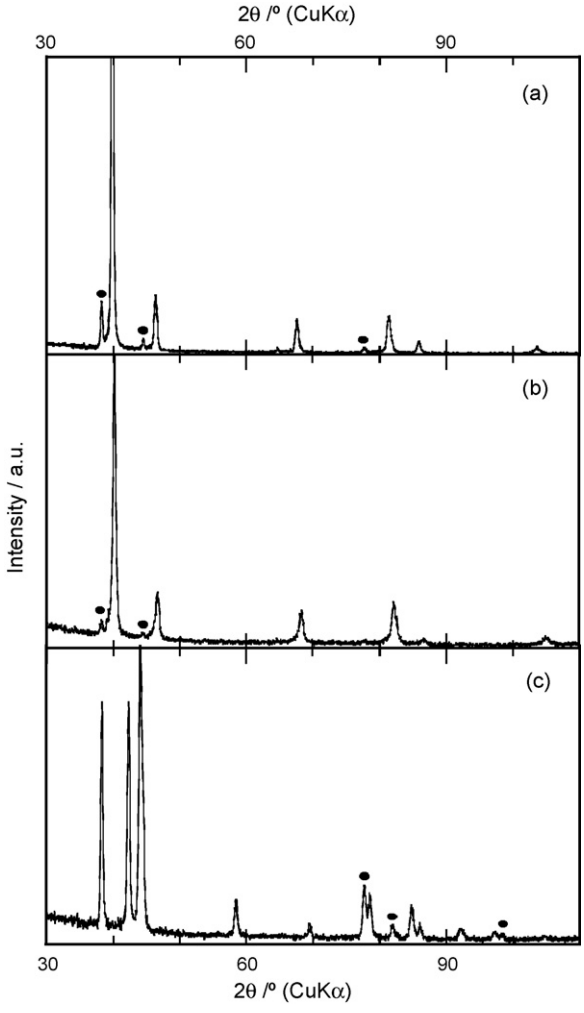

Fig. 2. XRD patterns of: (a) Pt, (b) $Pt_{50}Ru_{50}$, and (c) Ru on Au substrate prepared by sputtering technique at 600 °C.

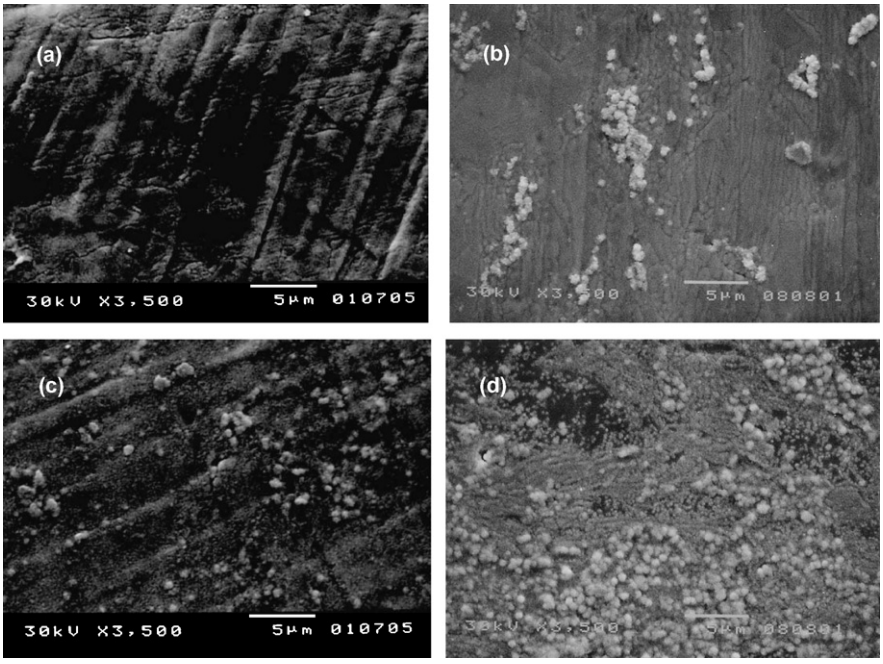

Fig. 3. SEM images of the sputtered Pt and Pt–Ru surfaces: (a) Pt, (b) $Pt_{15}Ru_{85}$, (c) $Pt_{50}Ru_{50}$, and (d) $Pt_{35}Ru_{65}$.

3. Results and discussion

3.1. Characterization of the sputter-deposited layers

Fig. 2 shows the X-ray diffraction (XRD) patterns of the sputter-deposited (a) Pt, (b) $Pt_{50}Ru_{50}$, and (c) Ru electrodes. Each diffraction peak was indexed by calculating an interplanar spacing [51]. All the diffraction peaks marked by the black dots correspond to the Au substrate. In Fig. 2(a), all the diffraction peaks based on Pt are indexed as a face centered cubic lattice (fcc); while in Fig. 2(c), all the Ru-based peaks are of a hexagonal close-packed structure (hpc). From these, the sputter-deposited electrocatalysts are found to be of a crystalline.

Fig. 2(b) shows an XRD pattern of the $Pt_{50}Ru_{50}$ layer. The diffraction angles are almost the same for Pt; although the peak angles are slightly shifted from those of Pt or Ru alone [52]. This suggests that Ru dissolves in Pt to form a Pt–Ru alloy with the fcc characteristics of Pt.

From the XRD results, the metallic bond radius of the Pt was calculated to be 1.39 Å, which well corresponds to that of 1.386 Å obtained by the lattice constant of 3.919 Å. As for $Pt_{50}Ru_{50}$, its lattice constant was found to be 3.891 Å, which is slightly smaller than that of Pt. The metallic bond radius of Ru is 1.33 Å, which is smaller than that of Pt. From these results, the peak shift observed in Fig. 2(b) is confirmed to be based on the Pt–Ru alloy formation.

Fig. 3 shows the surface SEM images of the sputtered Pt and Pt–Ru layer. From the figure, the Pt layer is known to have a uniform surface, whereas small grains are recognized for the Pt–Ru surface. The number and size of the grain increase according to an increase in the Ru content. The EPMA analysis revealed that the Pt component is larger at the top of the grain than at the other part.

Gasteiger et al. reported for their Pt–Ru alloy prepared by arc-fusing and post-annealing techniques that the same kind of Pt enriched surface is detected by an low-energy ion scattering (LEIS) measurement. Since the surface free energy of Pt is lower than that of Ru, they considered Pt preferentially gathered at the surface during a cool down after the post-anneal at 800 °C.

Our sputter-deposition was conducted at a substrate temperature of 600 °C. This process is likely to make it easy for generating a Pt-enriched part during the cooling step.

3.2. Electrochemical characteristics of the Pt and Pt–Ru in $HClO_4$

The background cyclic voltammograms of the Pt and Pt–Ru electrodes, measured in deaerated 0.5 mol dm^{-3} $HClO_4$ in the potential range of 0.0–0.7 V vs. RHE, are demonstrated in Fig. 4. Although the Ru dissolution takes place at 0.8–1.0 V vs. the RHE [53], the Pt–Ru electrodes are considered to be stable during the cyclic voltammetry measurement.

As for the cyclic voltammogram of the Pt electrode, proton adsorption/desorption peaks are observed in the potential range of 0.0–0.3 V vs. RHE, and an infinitesimal current is seen in the electrical double layer potential region of 0.3–0.7 V vs. RHE. These results ensure that the Pt surface is very pure in an electrochemical sense. Regarding the Pt–Ru voltammograms, the current density increases with an increase in the Ru content over the entire potential region. The current increase over 0.0–0.3 V vs. RHE which accompanies the disappearance of the proton adsorption/desorption peaks is based on the fact that the Ru-oxide is formed in the potential region [54].

To understand the current increase in the potential region of the electrical double layer, the ac impedance measurement was conducted at 0.5 V vs. RHE. Fig. 5 is the Cole–Cole plot of

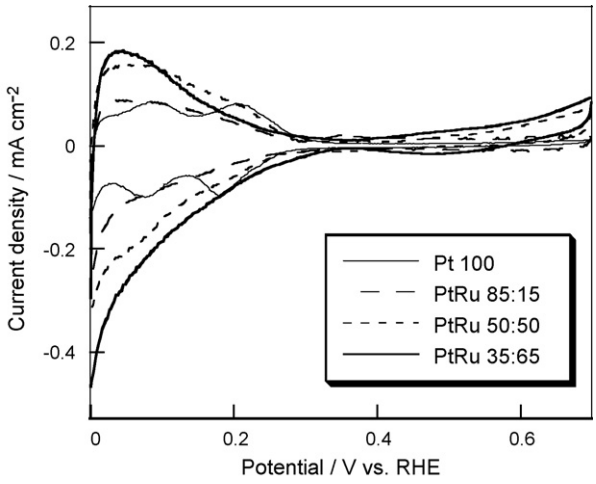

Fig. 4. Cyclic voltammograms measured in deaerated 0.5 mol dm^{-3} $HClO_4$ at Pt and Pt–Ru electrodes. Scan rate, 50 mV s^{-1}.

the Pt electrode taken in the frequency range of 10 kHz–1 Hz with an applied voltage of ±10 mV. The result shown in Fig. 5 points out that the equivalent circuit is expressed by a simple series connection of the solution resistance, R_s, and the double layer capacity, C_{dl}. The same kind of results is realized for the Pt–Ru electrodes. Inset of Fig. 5 illustrates the Ru content dependency of the C_{dl} magnitude, which is normalized by the apparent electrode area. It is known from the inset that the C_{dl} increases with an increase in the Ru content, and that the surface area of $Pt_{35}Ru_{65}$ is 3.5 times greater than that of Pt_{100}. Therefore, it is considered that the Pt–Ru surface area is enhanced by the grains observed in the SEM photographs of Fig. 3, in which the number and size of the grains increase with an increase in the Ru content.

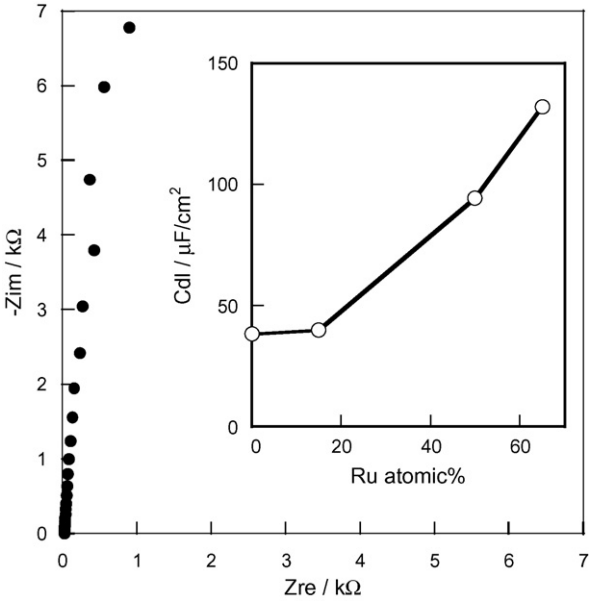

Fig. 5. Cole–Cole plot of the Pt electrode measured in 0.5 mol dm^{-3} $HClO_4$ at an electrode potential of 0.7 V vs. Ag/Ag_2SO_4. Inset shows the Pt–Ru composition dependence of the double layer capacitance.

Table 1
Temperature dependence of the inner cell pressure containing 0.5 mol dm^{-3} alcohol + 0.5 mol dm^{-3} $HClO_4$ aqueous solution

	Pressure (atm)			
	25 °C	50 °C	80 °C	100 °C
Methanol	1.00	1.16	1.55	2.12
2-Propanol	1.00	1.12	1.40	1.92

3.3. Methanol and 2-propanol oxidation at sputtered Pt electrode

First, by using the Pt electrode, the methanol and 2-propanol electrooxidation properties were measured by cyclic voltammetry in the above-mentioned gas-tight cell. The relationships between the temperature and inner pressure of the cell were measured and listed in Table 1.

Fig. 6 shows the CVs of the Pt electrode for the methanol and 2-propanol oxidation. In Fig. 6(a), at 25 °C, the methanol oxidation current peak is recorded at 0.9 V vs. RHE; while those of the 2-propanol oxidation are observed at 0.75 and 1.28 V vs. RHE. The onset potentials of methanol and 2-propanol are at 0.6 and 0.2 V vs. RHE, respectively. These data indicate that the overvoltage of the methanol oxidation is much higher than that of the 2-propanol oxidation. In addition, the peak current density is almost the same for the two alcohols.

Fig. 6(b)–(d) represent the CVs measured at 50, 80, and 100 °C, respectively. Based on the increase in the temperature, the difference in the onset potentials became smaller. At 80 and 100 °C, the onset potentials for the methanol and 2-propanol oxidations are almost the same. In addition, the methanol oxidation current density exceeds that of 2-propanol at 100 °C. These results suggest that methanol is preferentially used at 80–100 °C, and 2-propanol can be adapted for room temperature operation in DAFCs.

3.4. Methanol and 2-propanol oxidation at Pt–Ru electrodes

Fig. 7 shows the CVs of the methanol oxidation at the Pt and Pt–Ru electrodes at 25 and 100 °C. The methanol oxidation current density at the Pt–Ru is obviously higher than that of the Pt electrode, and the onset potential of the former is much more negative than that of the latter. The highest current density and the most cathodic onset potential are observed at the Pt:Ru = 50:50 electrode.

Fig. 8 shows the CVs of the 2-propanol oxidation at the sputtered electrodes at 25 and 100 °C. The current density of 2-propanol oxidation depends on the Pt–Ru composition, in which the maximum current density is recorded at Pt:Ru = 35:65 for each temperature. The open circuit potentials are found between 0 and 0.2 V vs. RHE, which shifts toward the cathodic direction with an increase in the Ru content. At the Pt:Ru = 50:50 and Pt:Ru = 35:65 electrodes, a current shoulder for the 2-propanol oxidation is seen around 0.1–0.3 V vs. RHE. The phenomenon is clearly observed at the higher temperature.

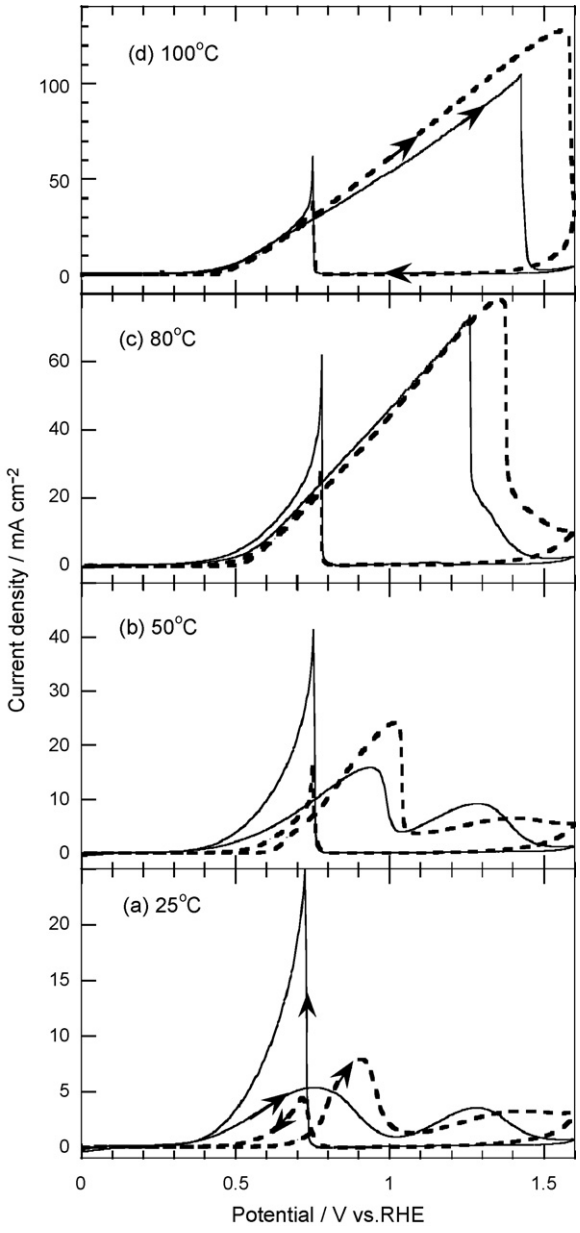

Fig. 6. Cyclic voltammograms of 0.5 mol dm^{-3} alcohol + 0.5 mol dm^{-3} $HClO_4$ at Pt electrode at: (a) 25 °C, (b) 50 °C, (c) 80 °C, and (d) 100 °C. Scan rate, 50 mV s^{-1}. Dashed curve: methanol; solid curve: 2-propanol.

Fig. 9 illustrates the Pt–Ru composition dependency of the current densities of the methanol and 2-propanol oxidations at 0.7 V vs. RHE. Based on the data taken at 25 and 50 °C, the 2-propanol oxidation current density exceeds that of the methanol oxidation. However, at 80 and 100 °C, the magnitude of the current density is almost the same except for the electrode composition of Pt:Ru = 35:65.

Based on these observations, the Pt–Ru electrode demonstrates a high catalytic activity for the 2-propanol oxidation as well as the methanol oxidation. The optimized composition was found to be Pt:Ru = 50:50 for the methanol oxidation and Pt:Ru = 35:65 for the 2-propanol oxidation, even when we consider the C_{dl} in terms of the surface area (see Fig. 5).

For methanol oxidation, Watanabe et al. reported that the optimized composition is Pt:Ru = 50:50 at the Pt–Ru alloy and the Pt–Ru loading carbon [6,55,56]. Gasteiger et al. used a bulk Pt–Ru alloy and reported the optimized composition of the Pt:Ru = 90:10 at 25 °C and Pt:Ru = 35:65 at 60 °C [54]. The present study demonstrated the highest current density and lowest overpotential at Pt:Ru = 50:50 in the temperature range of 25–100 °C.

3.5. Methanol electrooxidation mechanism

The reaction mechanism was then investigated on the basis of the Tafel plot analyses. Fig. 10 shows the Tafel plots for the methanol oxidation obtained by linear sweep voltammograms at the sweep rate of 1 mV s^{-1}.

Fig. 10(A) shows the Tafel plots of the methanol oxidation at the Pt electrode. The main slope is 89 mV decade^{-1} at 25 °C and 81 mV decade^{-1} at 100 °C. If it is assumed that the transfer coefficient α is 0.5, the number of electrons involved in the electrode reaction n is 1.33 at 25 °C and 1.83 at 100 °C.

For the case of the Pt:Ru = 50:50 electrode, the Tafel slope is estimated, in the same manner as for the Pt electrode, to be 87 mV decade^{-1} at 25 °C and 76 mV decade^{-1} at 100 °C as

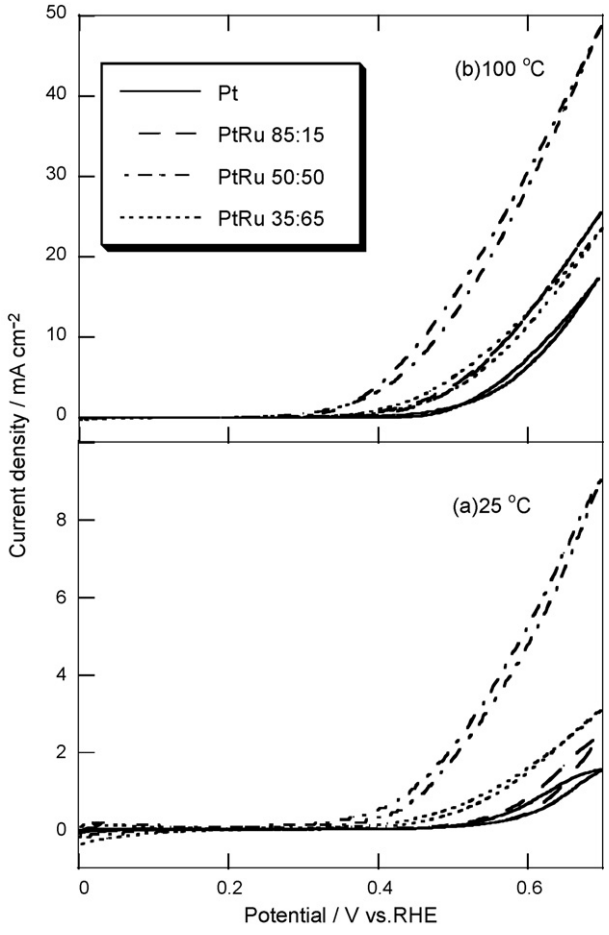

Fig. 7. Cyclic voltammograms of 0.5 mol dm^{-3} methanol + 0.5 mol dm^{-3} $HClO_4$ at Pt–Ru electrode at (a) 25 °C and (b) 100 °C. Scan rate, 50 mV s^{-1}.

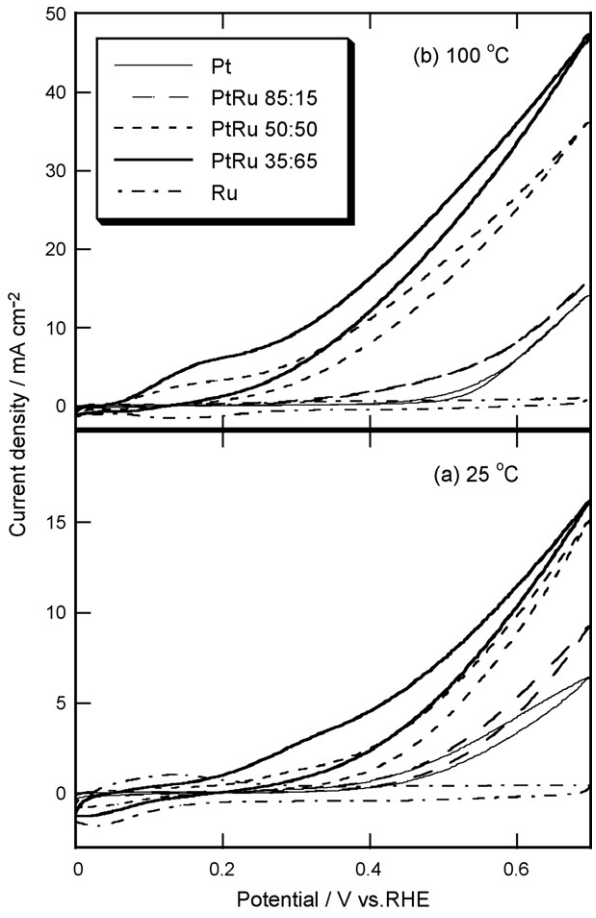

Fig. 8. Cyclic voltammograms of 0.5 mol dm^{-3} 2-propanol + 0.5 mol dm^{-3} $HClO_4$ at Pt–Ru electrode at (a) 25 °C and (b) 100 °C. Scan rate, 50 mV s^{-1}.

seen in Fig. 10(B). Therefore, one obtains $n = 1.36$ at 25 °C and $n = 1.95$ at 100 °C.

Inada et al. reported the Tafel slope of the methanol oxidation at the Pt electrode to be 90–100 mV decade^{-1} in the potential range of 0.55–0.7 V vs. RHE at room temperature [57], which well agrees with the results of Fig. 10. Thus, it is postulated that $n \approx 1$ at 25 °C and $n \approx 2$ at 100 °C. The methanol electrooxidation pathway is considered as follows [57,58]:

$$Pt + CH_3OH \rightarrow Pt(CH_3OH)_{ads} \quad (1)$$

$$Pt(CH_3OH)_{ads} \rightarrow Pt(CH_{4-n}O) + nH^+ + ne^- \quad (2)$$

$$M + H_2O \rightarrow M\text{–}OH + H^+ + e^- \quad (3)$$

$$Pt\text{–}CO + M\text{–}OH \rightarrow CO_2 + H^+ + e^- \quad (4)$$

$$Pt\text{–}CO + H_2O \rightarrow CO_2 + 2H^+ + 2e^- \quad (5)$$

It is known that the methanol dissociative adsorption expressed by Eqs. (1) and (2) occurs around 0.1–0.3 V vs. RHE at Pt and Pt–Ru [59,60]. In Fig. 10, the Tafel slope is observed at 0.45–0.65 V vs. RHE at 25 °C, hence the rate-determining process does not include the reaction depicted by Eq. (2). Therefore, the rate-determining process at 25 °C is considered to be Eq. (3) or (4); although, Eq. (3) is reported to be the rate determining one by many workers [59,61,62].

When we look at Fig. 10 again, the current-potential characteristics at 25 and 100 °C are completely different. At 25 °C, the main slope appeared after an induction current; whereas, at 100 °C, the Tafel slope dramatically shifts in the cathodic direction and does not accompany any induction current. These results strongly indicate that the rate-determining process of the methanol oxidation is different at 25 and 100 °C. Thus, the rate-determining process at 100 °C is believed to be Eq. (5) which involves a two electron transfer.

3.6. 2-Propanol electrooxidation mechanism

Fig. 11(A) shows the Tafel plots of the 2-propanol oxidation at the Pt electrode. The slopes observed at the low potentials of 0.25–0.4 V vs. RHE are 125 mV decade^{-1} at 25 °C and 165 mV decade^{-1} at 100 °C. When we assume that the transfer coefficient α is 0.5, the number of electrons involved in the electrode reaction n is 0.95 at 25 °C and 0.9 at 100 °C. At

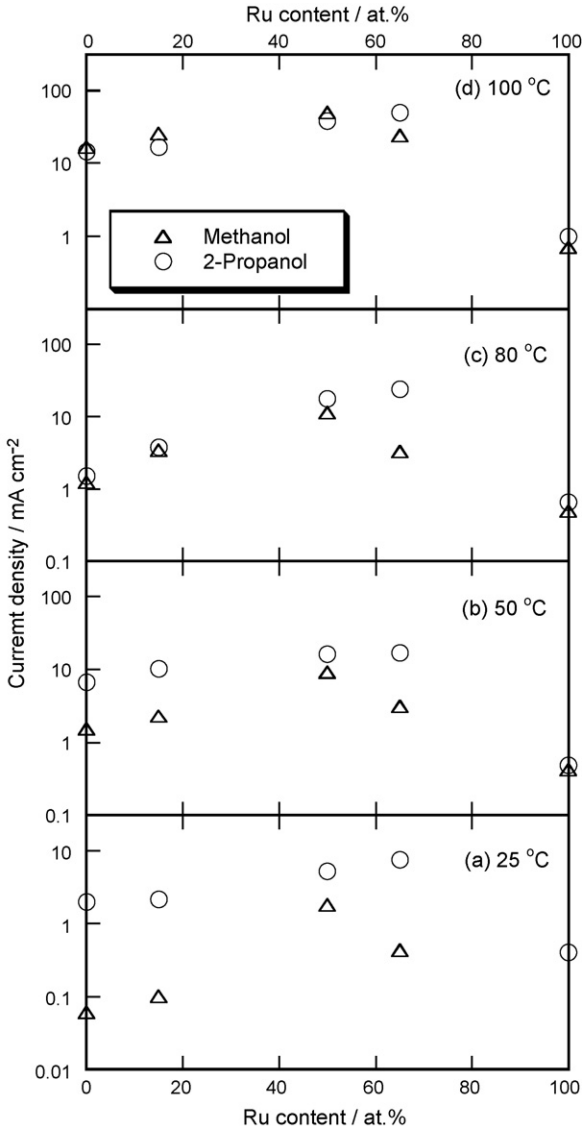

Fig. 9. Pt–Ru composition dependence of methanol and 2-propanol oxidation current density at 0.7 V vs. RHE.

high potentials, the slopes are 245 mV decade^{-1} at 25 °C and 220 mV decade^{-1} at 100 °C. These high values imply that the oxidation reaction involves the 2-propanol diffusion process at high potentials.

In the case of the Pt:Ru = 50:50 electrode, Tafel slopes of 129, 189 and 454 mV decade^{-1} at 25 °C and 156, 89 and 437 mV decade^{-1} at 100 °C are observed in Fig. 11(B). In the same manner, in the low-potential region, one obtains $n = 0.92$ at 25 °C and $n = 0.95$ at 100 °C. The Tafel slopes at the high potentials are thought to be influenced by the diffusion process in the same way.

Based on these results, the number of electrons transferred by the rate-determining process is supposed to be one in the low-current region. Pastor et al. detected acetone and CO_2 as the reaction products of the 2-propanol electrooxidation using differential electrochemical mass spectrometry (DEMS) and Fourier transform IR spectroscopy (FTIR) [48]. Rodrigues et al. found acetone at an electrode potential less than 0.9 V vs. RHE and CO_2 at much more positive potentials [49]. We have previously reported that only acetone is detected as a reaction product during the direct 2-propanol single cell operation [50].

When we consider the fact that the main product of the 2-propanol oxidation in the fuel cell is acetone, the reaction pathway is postulated to the following Eqs. (6) and (7), which involves the rate-determining process of a 1-electron transfer

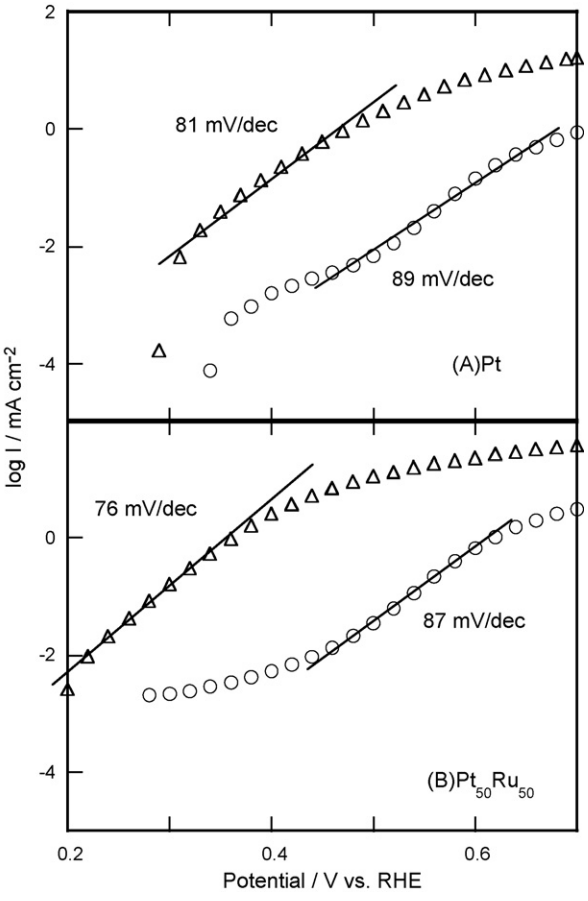

Fig. 10. Tafel plots of methanol oxidation at (A) Pt and (B) Pt:Ru = 50:50 electrodes. Temperature: 25 °C (circles) and 100 °C (triangles).

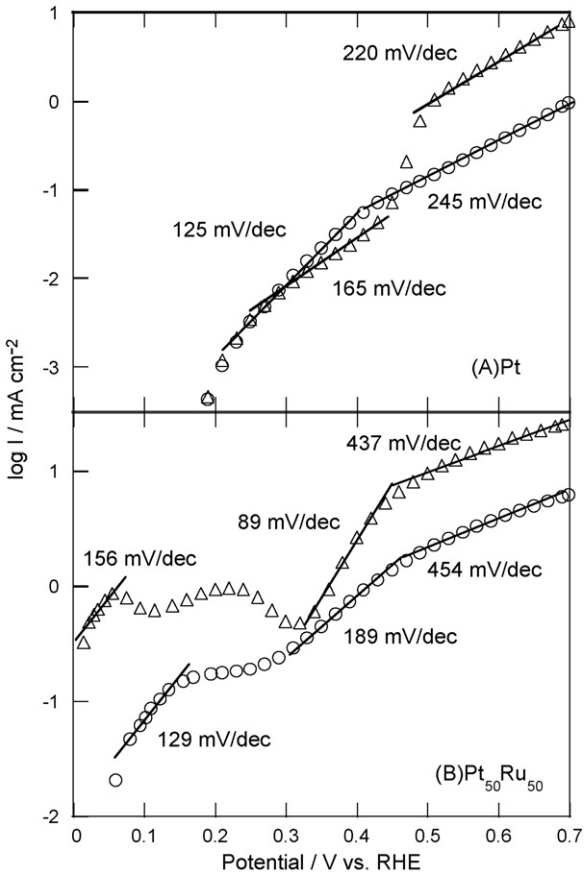

Fig. 11. Tafel plots of 2-propanol oxidation at (A) Pt and (B) Pt:Ru = 50:50 electrodes. Temperature: 25 °C (circles) and 100 °C (triangles).

that accompanies the proton-elimination reaction.

$$CH_3CHOHCH_3 \rightarrow CH_3COHCH_3 + H^+ + e^- \quad (6)$$

$$CH_3COHCH_3 \rightarrow CH_3COCH_3 + H^+ + e^- \quad (7)$$

However, we cannot presently decide whether Eq. (6) or Eq. (7) is the rate-determining step.

4. Conclusions

The electrooxidation properties of methanol and 2-propanol, which are both promising candidates for DAFCs, were studied under elevated temperature and pressurized conditions. Sputter-deposited Pt and Pt–Ru electrodes were well-characterized and utilized for the electrochemical measurement of alcohol oxidation at 25–100 °C. The prepared Pt electrode at 600 °C had a flat surface, and the Pt–Ru formed an alloy. The electrochemical measurements were carried out in a gas-tight cell at elevated temperature, which accompanies the pressurized condition. This is representative of the DAFC rising temperature operation.

As a result, at 25 °C, the onset potential of the 2-propanol oxidation is about 400 mV more negative than that of the methanol oxidation, and the current density of the 2-propanol oxidation exceeds that of the methanol oxidation. Conversely, at 100 °C, the methanol oxidation current density overcomes that of the 2-propanol, and the onset potentials of the two are almost

the same. The highest current density for the methanol oxidation is obtained at the Pt:Ru = 50:50 electrode, whereas at the Pt:Ru = 35:65 for the 2-propanol oxidation.

Tafel plot analysis was used to investigate the reaction mechanism. For the methanol oxidation, the number of electrons transferred during the rate-determining process was estimated to be 1 at 25 °C and 2 at 100 °C. This suggests that the reaction mechanism differs at 25 and 100 °C. In contrast, the rate-determining process of the 2-propanol oxidation at 25 and 100 °C was expected to be a 1-electron transfer which accompanies the proton-elimination reaction to produce acetone.

Consequently, it is deduced that methanol and 2-propanol have an advantage during the rising temperature and room temperature operation, respectively.

Acknowledgment

The present study was financially supported by a Grant-in-Aid for Scientific Research (B) (No. 16350098) from the Ministry of Education, Culture, Sports, Science and Technology (MEXT), Japan.

References

[1] R. Dillon, S. Srinivasan, A.S. Aricò, V. Antonucci, in: N. Brandon, D. Thompsett (Eds.), Fuel Cells Compendium, Elsevier, Amsterdam, 2005 (Chapter 10).
[2] D.C. Dunwoody, H. Chung, L. Haverhals, J. Leddy, in: S. Minteer (Ed.), Alcoholic Fuels, Taylor & Francis, Boca Raton, 2006 (Chapter 9).
[3] Y.-S. Kim, B.S. Pivovar, in: T.S. Zhao, K.-D. Kreuer, T.V. Nguyen (Eds.), Advances in Fuel Cells, Elsevier, Amsterdam, 2007 (Chapter 4).
[4] G.T. Burstein, C.J. Barnett, A.R. Kucernak, K.R. Williams, Catal. Today 38 (1997) 425.
[5] A.B. Anderson, E. Grantscharova, S. Seong, J. Electrochem. Soc. 143 (1996) 2075.
[6] M. Watanabe, S. Motoo, J. Electroanal. Chem. 60 (1975) 267.
[7] A. Hamnett, Catal. Today 38 (1997) 445.
[8] S. Wasmus, A. Kuver, J. Electroanal. Chem. 462 (1999) 14.
[9] Y. Tong, H.S. Kim, P.K. Babu, P. Waszczuk, A. Wieckowski, E. Oldfield, J. Am. Chem. Soc. 124 (2002) 468.
[10] A. Kabbabi, R. Faure, R. Durand, B. Beden, F. Hahn, J.-M. Lever, C. Lamy, J. Electroanal. Chem. 444 (1998) 41.
[11] H. Wang, C. Wingender, H. Baltruschat, M. Lopez, M.T. Reetz, J. Electroanal. Chem. 509 (2001) 163.
[12] J.-M. Leger, J. Appl. Electrochem. 31 (2001) 767.
[13] K. Kwang, H.A. Gasteiger, N.M. Markovic, P.N. Ross, Electrochim. Acta 41 (1996) 2587.
[14] P. Waszczuk, G.-Q. Lu, A. Wieckowski, C. Lu, C. Rice, R.I. Masel, Electrochim. Acta 47 (2002) 3637.
[15] H.A. Gasteiger, N. Markovic, P.N. Ross, E.J. Cairns, Electrochim. Acta 39 (1994) 1825.
[16] A. Hamnett, in: A. Wieckowski (Ed.), Interfacial Electrochemistry: Theory, Experimental and Applications, Marcel Dekker, New York, 1999.
[17] A. Lima, C. Coutanceau, J.M. Léger, C. Lamy, J. Appl. Electrochem. 31 (2001) 379.
[18] M. Gotz, H. Wendt, Electrochim. Acta 43 (1998) 3637.
[19] A.S. Arico, Z. Poltarzewski, H. Kim, A. Morana, N. Giordano, V. Antonucci, J. Power Sources 55 (1995) 159.
[20] A.S. Arico, P. Creti, N. Giordano, V. Amtpmicci, J. Appl. Electrochem. 26 (1996) 959.
[21] C. He, H.R. Kunz, J.M. S Fenton, Electrochemical Society Proceedings PV 97-13, Pennington, NJ, 1997, p. 52.
[22] P.K. Shen, A.C.C. Tseung, J. Electrochem. Soc. 141 (1994) 3082.
[23] P. Shen, K. Chen, A.C.C. Tseung, J. Chem. Soc., Faraday Trans. 90 (1994) 3089.
[24] A. Gamnett, B.J. Kennedy, S.A. Weeks, J. Electroanal. Chem. 240 (1988) 349.
[25] A.C.C. Tseung, K.Y. Chen, Catal. Today 38 (1997) 439.
[26] P.J. Kulesza, L.R. Faulkner, J. Electroanal. Chem. 259 (1989) 81.
[27] M. Krausa, W. Vielstich, J. Electroanal. Chem. 379 (1994) 307.
[28] T. Frelink, W. Visscher, A.P. Cox, J.A.R. Van Veen, Electrochim. Acta 40 (1995) 1537.
[29] S.C. Gebhard, R.G. Windham, B.E. Koel, J. Phys. Chem. 94 (1990) 6831.
[30] Y. Ishikawa, M. Liao, C.R. Cabrera, Surf. Sci. 463 (2000) 66.
[31] S. Mukerjee, S.J. Lee, E.A. Ticianelli, J. McBreen, B.N. Grgur, N.M. Markoviæ, P.N. Ross, J.R. Giallombardo, E.S. De Castro, Electrochem. Solid-State Lett. 2 (1999) 12.
[32] G. Samjeske, H. Wang, T. Löffer, H. Baltruschat, Electrochim. Acta 47 (2002) 3681.
[33] B.N. Grgur, G. Zhuang, N.M. Markoviæ, P.N. Ross, J. Phys. Chem. B 101 (1997) 3910.
[34] B.N. Grgur, N.M. Markoviæ, P.N. Ross, J. Phys. Chem. B 102 (1998) 2494.
[35] K. Lasch, L. Jorissen, J. Garche, J. Power Sources 84 (1999) 225.
[36] N. Markoviæ, P.N. Ross, J. Electroanal. Chem. 330 (1992) 499.
[37] W. Yang, D. Jaramillo, J.J. Gooding, D.B. Hibbert, R. Zhang, G.D. Willett, J. Fisher, Chem. Commun. (2001) 1982.
[38] I. Rubinstein, S. Steinberg, Y. Tor, A. Shanzer, J. Sagiv, Nature 332 (1988) 31.
[39] M. Umeda, H. Ojima, M. Mohamedi, I. Uchida, J. Power Sources 136 (2004) 10.
[40] DOE/NETL, Fuel Cell Handbook, 7th ed., EG&G Technical Services, Morgantown, 2004 (Chapter 3).
[41] I.A. Rodrigues, J.P.I. De Souza, E. Pastor, F.C. Nart, Langmuir 13 (1997) 6829.
[42] S.-G. Sun, Y. Lin, Electrochim. Acta 41 (1996) 693.
[43] E. Pastor, S. Gonzalez, A.J. Arvia, J. Electroanal. Chem. 395 (1995) 233.
[44] N. Fujiwara, Z. Siroma, T. Ioroi, K. Yasuda, J. Power Sources 164 (2007) 457.
[45] Z. Qi, M. Hollett, A. Attia, A. Kaufman, Electrochem. Solid-State Lett. 5 (2002) A129.
[46] Z. Qi, A. Kaufman, J. Power Sources 118 (2003) 54.
[47] D. Cao, S.H. Bergens, J. Power Sources 124 (2003) 12.
[48] E. Pastor, S. Gonzalez, A.J. Arvia, J. Electroanal. Chem. 365 (1995) 233.
[49] A. Rodrigues, I. de Souza, E. Pastor, F.C. Nart, Langmuir 13 (1997) 6829.
[50] M. Umeda, M. Sugii, M. Mohamedi, I. Uchida, Electrochemistry 70 (2002) 916.
[51] A.R. West, Basic Solid State Chemistry, Wiley, Tokyo, 1996.
[52] E. Antolini, F. Cardelloni, J. Alloys Compd. 313 (2001) 118.
[53] K.L. Ley, R. Liu, C. Pu, Q. Fan, N. Leyarovska, C. Segre, E.S. Smotkin, J. Electrochem. Soc. 144 (1997) 1543.
[54] H.A. Gasteiger, N. Markovic, P.N. Ross, E.J. Cairns, J. Phys. Chem. 97 (1993) 12020.
[55] S. Motoo, M. Watanabe, J. Electroanal. Chem. 69 (1976) 429.
[56] M. Watanabe, M. Uchida, S. Motoo, J. Electroanal. Chem. 229 (1986) 195.
[57] R. Inada, K. Shimazu, H. Kita, J. Electroanal. Chem. 277 (1990) 315.
[58] L.D. Burke, J.K. Casey, Electrochim. Acta 37 (1992) 1817.
[59] T. Iwashita, Electrochim. Acta 47 (2002) 3663.
[60] K. Kashima, M. Umeda, A. Yamada, I. Uchida, Electrochemistry 74 (2006) 166.
[61] Y. Zhu, H. Uchida, T. Yajima, M. Watanabe, Langmuir 17 (2001) 146.
[62] M. Umeda, M. Kokubo, M. Mohamedi, I. Uchida, Electrochim. Acta 48 (2003) 1367.